

Production of Deeply Ionized Super Heavy Ions from Ultraintense Laser-Driven Plasma

Pengjie Wang¹, Zheng Gong¹, Seong Geun Lee^{2,3}, Yinren Shou¹, Yixing Geng¹, Cheonha Jeon², I Jong Kim⁴, Hwang Woon Lee², Jin Woo Yoon^{2,5}, Jae Hee Sung^{2,5}, Seong Ku Lee^{2,5}, Defeng Kong¹, Jianbo Liu¹, Zhusong Mei¹, Zhengxuan Cao¹, Zhuo Pan¹, Il Woo Choi^{2,5¶}, Xueqing Yan^{1†}, Chang Hee Nam^{2,3‡}, Wenjun Ma^{1*}

¹*State Key Laboratory of Nuclear Physics and Technology, School of Physics & CAPT, Peking University, Beijing, China*

²*Center for Relativistic Laser Science, Institute for Basic Science, Gwangju 61005, Korea*

³*Department of Physics and Photon Science, Gwangju Institute of Science and Technology, Gwangju 61005, Korea*

⁴*Center for Scientific Instrumentation, Korea Basic Science Institute, Daejeon 34133, Korea*

⁵*Advanced Photonics Research Institute, Gwangju Institute of Science and Technology, Gwangju 61005, Korea*

We report the experimental generation of deeply ionized super-heavy ions (Au) with unprecedented energy of 1.2 GeV utilizing petawatt femtosecond laser pulses at the intensity of 10^{22} W/cm². A novel self-calibrated diagnostic method is developed to acquire the absolute energy spectra and charge state distributions of Au ions abundant at the charge state of 51+ and reaching up to 61+. Particle-in-cell simulations support that the laser intensity is the crucial parameter for the ionization dynamics and acceleration of Au ions over the pulse duration. Our results will trigger the generation of 10s GeV super-heavy ions and advancement of diagnostic methods, which are important for applications, such as injectors for heavy ion accelerator, heavy ion fusion, and generation of warm dense matter.

The generation of energetic ions from laser-irradiated targets has been an attractive topic[1-3] in the past two decades, owing to the unique features such as ultra-high accelerating gradient, micrometer-scale source size, high beam density and low emittance[4-6]. In particular, laser-driven super-heavy ion (mass number ~ 200) source is ideally suited for applications to fission-fusion reaction[7], high-energy-density physics[8], or as injectors for high-energy accelerators[9]. Compared with the acceleration of low-Z ions (80 MeV/nucleon for C) and mid-Z ions (10-20 MeV/nucleon for Al, Fe and Ag)[4,10-13], the energy of super-heavy ions (SHIs) generated from laser-plasma interactions is quite low all the time. For example, 2 MeV/nucleon of Pb[14] and 5 MeV/nucleon of Au[15] ions were reported by employing 100 J-class lasers, which is unfeasible for applications that need high-repetition rate and high average flux.

Generally, the acceleration of SHIs would be suppressed by the inevitable contamination attached to the surface of solid targets, where the undesired hydrocarbons are more readily accelerated due to their higher charge-to-mass ratio. Resistive heating[16] or laser heating[17] have been proven as useful methods of removing the contamination and thus weakening the suppression effect. However, SHIs is still hard to be efficiently accelerated, because they can't be ionized to high charge states and experience a long acceleration time[18]. The accessible intensity of 10^{20} W/cm² for picosecond laser pulses,

widely utilized for the acceleration of low-Z and mid-Z ions, is insufficient to collisionless deeply ionize SHIs. Compared with femtosecond lasers, collisional ionization by picosecond lasers requires the deposition of higher laser energy in plasma, but resulting in the lower scaling factor of the maximum energy of SHIs with laser energy[19]. When a femtosecond laser pulse irradiates an ultra-thin target[5], huge ponderomotive force can pile up bulk electrons to build up an ultra-strong charge separation field, resulting in deep collisionless ionization[20] and prompt injection[21]. It has been predicted, upon the coming petawatt and exawatt class laser facilities[22], that 10s GeV thorium (²³²Th) ions with very high charge states can be obtained[23] at the intensity of 10^{23} W/cm². The state-of-art multi-petawatt femtosecond lasers[24] are capable of delivering an intensity higher than 10^{22} W/cm². However, the proof-of-principle experiment on highly charged super-heavy ion source, driven by the femtosecond laser pulses at such ultra-high intensity, has not yet been demonstrated so far.

In this Letter, we report an experimental study on the generation of deeply ionized energetic Au ions by employing ultra-intense femtosecond laser pulses at the intensity of 10^{22} W/cm². Au ions with the maximum charge state of 61+ and the maximum energy of 1.2 GeV were obtained. The particle-in-cell (PIC) simulations reveal how the maximum energy of the Au ions depends on the laser intensity over the

pulse duration throughout examining the transverse-position-dependent ionization process. We develop a self-calibrated diagnostic method of measuring the absolute energy spectra and charge state distributions of Au ions unambiguously, which can be used as a diagnostic tool of the acceleration field and the laser intensity. In our experiments, charge state distributions from single and double-layer targets indicate that the maximum acceleration field strengths are similar, which then imply the energy enhancement in double-layer targets is mainly due to the prolongation of the acceleration time, in good agreement with PIC simulations.

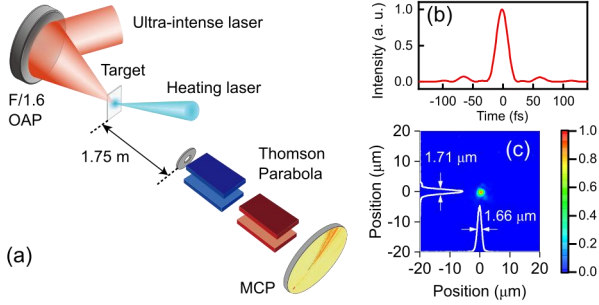


FIG. 1. (a) Experimental setup. The temporal profile (b) and the focal spot (c) of driving laser pulses.

The experiments were carried out in the 4 petawatt Ti:sapphire laser facility[25] located at the Center for Relativistic Laser Science (CoReLS). The p-polarized laser pulses were tightly focused onto targets by an f/1.6 off-axis parabolic mirror with the energy of 14-15 J as shown in Fig. 1(a). The temporal profile of the pulse was measured with a SPIDER right after the pulse compressor. The full-width-at-half-maximum (FWHM) duration was 22 fs as shown in Fig. 1 (b). The focal spot characterization was performed with a pair of lenses and a 12-bit CMOS camera in the 100 TW mode by attenuating the beam with partial reflection mirrors[24]. Fig.1(c) shows the measured focal spot. The best focal spot size measured in the campaign had a near-diffraction-limited size of $1.71 \times 1.66 \mu\text{m}^2$ FWHM, and 32% of the laser energy was concentrated in the FWHM area. Calculated from the pulse duration and focal spot measurement and taking into account of the fluctuation in the focal spot quality, the on-target intensity was $1.1 \pm 0.4 \times 10^{22}$ W/cm², which corresponds to a normalized laser amplitude of $a_0 = eE_0/mc\omega \approx 57-84$, where e , m , c , ω , and E_0 is electron charge, mass, light speed, laser frequency, and electric field amplitude, respectively. The contrast ratio of the laser pulse was better than 10^{12} up to 2 ps before the main pulse by employing a double plasma mirror system, which avoids the prepulse-heating and premature expansion of the targets happened for low-contrast laser[12]. Single-layer targets made of ultra-thin Au foils, and double-layer targets composed of near-critical-density (NCD) carbon nanotube foams (CNF)[13]

and ultra-thin Au foils, were used in the experiments. The density of the CNF is $2.3 \pm 0.5 \text{ mg/cm}^3$, corresponding to electron density of $0.4 \pm 0.1 n_c$ when the atoms are fully ionized, where $n_c = m\omega^2\epsilon_0/e^2$ is the critical density of the plasma. The laser pulse was focused onto the CNF side with an incident angle of 2.5° . A continuous wave diode laser with the maximum power of 500 mW was utilized to heat the rear surface of targets to remove the contamination layer before the main laser irradiation. Ions were detected by a Thomson parabola spectrometer (TPS) equipped with a microchannel plate (MCP) with a phosphor. Ions hitting on the MCP assembly will produce optical signals which are imaged by a 16-bit charge-coupled device (CCD) camera. In order to acquire the charge state distribution (CSD) of Au ions, the TPS was placed 1.75 m away from the targets, and the diameter of the collimating pinhole is 310 μm , which results in an ultra-small detection solid angle of 2.47×10^{-8} sr. Only a few hundreds of Au ions can pass the pinhole and arrive at the MCP. A maximum electric field of 18.2 kV/cm was applied in TPS to disperse the Au ions as much as possible on the MCP to produce single-ion events.

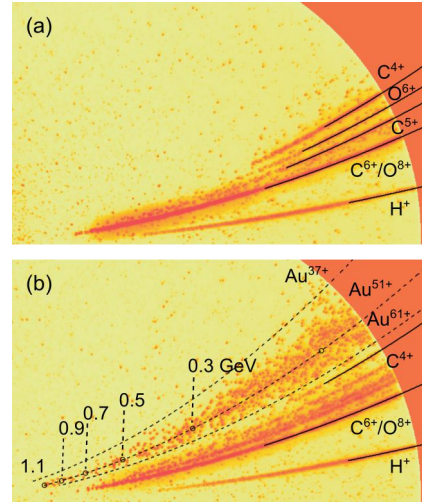


FIG. 2. TP images from (a) a 20-nm DLC target and (b) a double-layer Au target.

Fig. 2(a) and 2(b) show the raw Thomson parabola (TP) images from a 20-nm diamond-like carbon (DLC) and a double-layer Au target (60 μm CNF+150nm Au), respectively. In the TP image, ions with the same charge-to-mass ratio (CMR) are located in an identical parabola trace. For the DLC target, the traces of H^+ , $\text{C}^{6+}/\text{O}^{8+}$, C^{5+} , O^{6+} , and C^{4+} can be clearly distinguished. C and O ions with $\text{CMR} < 1/3$ are not observed, which indicates the acceleration of $\text{C}^{<4+}$ and $\text{O}^{<6+}$ are insignificant at this intensity. Based on this observation, we conclude that the cluster signals in the region of $\text{CMR} < 1/3$ for double-layer Au targets are caused only by the Au ions. As shown in Fig. 3(a), the clusters have similar shapes and clear boundaries, indicating they come from single-ion events. We

summed the CCD counts for each distinct cluster as the response of a single ion, and did the statistics as a function of the ion energy. The histogram of the responses collected in the region of $\text{CMR} < 1/3$ from multiple shots is shown in Fig. 3(b). The responses demonstrate a clear dependence on the energy of Au ions, as depicted in Fig. 3(c). We performed a series of calculations to simulate the MCP response curve considering the energy, incident angle, and incident positions of the ions (see Supplemental Material) [26]. The simulations agree well with the experimental results, confirming each cluster as the response of a single ion. At the bottom of Fig. 3(b), the responses of clusters outside of the Au ion region are also presented, as the background signal. They might come from other scattered radiations hitting on the MCP, of which counts are significantly lower than that of the ions.

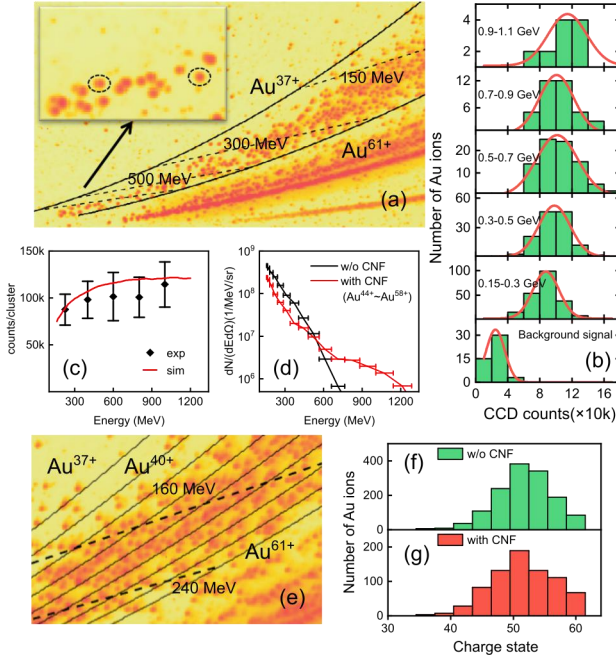


FIG. 3. (a) TP image from a double-layer Au target. The solid lines represent the parabolas of Au^{37+} and Au^{61+} , and the dashed lines represent the constant energy lines. The inset shows the zoomed clusters of ion signals. (b) Statistical results of single-ion events. The red lines are the Gaussian fitting curves. (c) Responses for Au ions. (d) Energy spectra of Au ions. (e) Schematic of the statistics of the CSD: solid lines represent the constant charge-state lines. CSD of Au ions from a single-layer (f) and a double-layer (g) targets.

Based on the obtained calibration, the absolute energy spectra and CSD of Au ions can be extracted. Figure 3(d) shows the energy spectra. The maximum Au energy from 150-nm single-layer targets is 710 MeV (3.6 MeV/nucleon), 3.6 times higher than the previous results obtained from 14 nm Au foils irradiated by femtosecond lasers[2]. For the double-layer target, the maximum Au energy is 1.2 GeV

(6.1 MeV/nucleon), enhanced by 1.5 times compared to single-layer target. The absolute CSD was obtained by counting the Au ions in striped areas segmented by the constant charge-state lines shown in Fig. 3(e). Technically, all CCD counts in one striped area, were summed after subtracting the background, and then were divided by the calibrated response of Au ions to obtain the ion numbers in that area. Limited by the resolution of TPS, the statistic division of charge states is set to be 3 in Figs. 3(f) and 3(g) for a clear observation of the trend. It is found that there are no significant differences between the cases of single-layer and double-layer targets, which will be analyzed below with the help of numerical simulations. By carefully examining the data, we conclude that highly charged state of up to 61+ (Ar-like Au ion) was obtained, and the abundant state is 51+ (Ni-like Au ion).

We performed a series of 2D PIC simulations to illustrate the ionization and acceleration process utilizing the EPOCH code[27]. The simulation region with a size of $90 \lambda_0 \times 30 \lambda_0$ is uniformly divided into 9000×3000 mesh grids. A linearly polarized laser with wavelength $\lambda_0 = 0.8 \mu\text{m}$ is incident from the left boundary with FWHM diameter of $1.69 \mu\text{m}$ and FWHM duration of 20 fs. A uniform 150-nm Au target with an atom density of $n_a = 5.96 \times 10^{28}/\text{m}^3$ is placed at $0 < x < 150 \text{ nm}$. In the case of the double-layer target, a NCD plasma slab (representing the CNF) with electron density of $0.4 n_c$ is placed ahead of the Au target. Here, both carbon and Au targets are initialized as neutral atoms[28], and are gradually ionized by the incident laser pulses. The field ionization model adopts the ADK ionization rate[29] where the equation is averaged over all possible magnetic quantum numbers. The corrected effect from barrier-suppression ionization is incorporated into ADK ionization rate as well[30]. Collisional ionization is not included in the simulation considering the ultra-thin thickness of the targets, and the high contrast and ultra-short duration of the driving pulse.

The spatial distribution of Au ions at $t = 146 \text{ fs}$ for the single-layer target irradiated by a laser pulse of $a_0 = 60$ is shown in Fig. 4(a). At this moment, the intensity peak of the laser pulse has been reflected for 87 fs from $t = 59 \text{ fs}$, and the primary acceleration process is completed. Ions near the center of the focus spot have higher charge states than those away from the center, as a consequence of the intensity gradient of the driving laser. Judging from their x positions, one can find that $\text{Au}^{\geq 51+}$ are more energetic than $\text{Au}^{< 51+}$. They are ionized in the strongest sheath field and accelerated with higher field gradients due to their higher CMR.

For the investigation of the acceleration process, the evolution of the charge states and the longitudinal momentum of Au ions, grouped according to their transverse positions, are examined, as shown in Fig. 4(b). Ions at the center of the focus

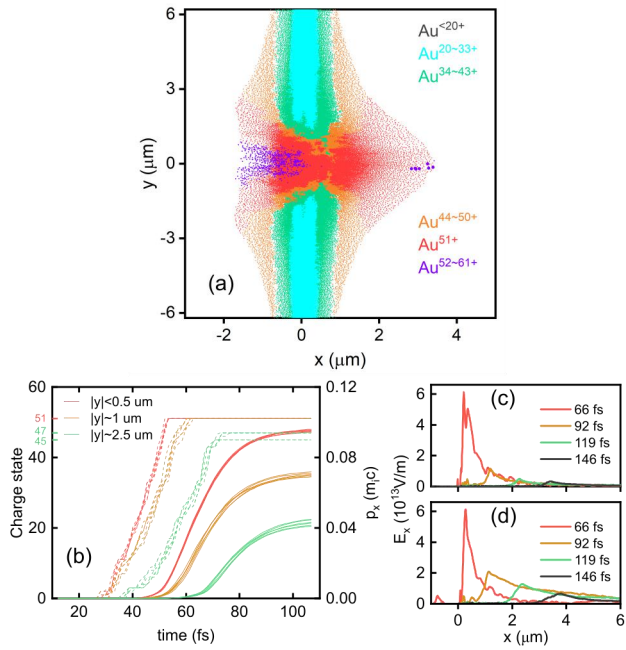


FIG. 4. (a) Spatial distribution of Au ions from a 150-nm single layer Au target for $a_0 = 60$ at $t = 146$ fs. (b) Evolution of the charge states (dashed lines) and the longitudinal momentum p_x (solid lines) of Au ions originating from different transverse positions $|y|$ for the target in (a): each line represents one macro-particle. Evolution of the acceleration field E_x for the single-layer target (c) and the double-layer target (d).

($|y| < 0.5 \mu\text{m}$, red lines) are firstly ionized to Au^{51+} , then undergo the longest acceleration time starting from $t = 45$ fs. Ions near the edge of the focus spot ($|y| \approx 1 \mu\text{m}$, yellow lines) are ionized to Au^{51+} 10 fs later, and their final energy is significantly lower. If ions originate further away from the center of the focus ($|y| \sim 2.5 \mu\text{m}$, green lines), they reach their final charge states (45-47) even later, which leads to a more inefficient acceleration as compared to those from the center of the focus spot.

The reason for the enhanced acceleration for double-layer targets was explored through PIC simulations. As shown from the temporal evolution of the acceleration field at $y = 0$ for the single-layer and double-layer targets, in Figs. 4(c) and 4(d), respectively, the maximum field strengths for the two cases are similar, but the acceleration field of the double-layer target decays much more slowly. This is due to the fact that the ions from double-layer targets undergo a second-stage acceleration boosted by the superponderomotive electrons from the CNF layer[13]. Eventually, they gain higher energy due to the prolonged acceleration time.

Instead of using the double-layer targets, the acceleration time can be prolonged by experimentally stretching the driving pulses as well, which nevertheless would lead to the reduction of laser intensity for a given laser energy. For low- Z

ions, it was found that the optimal pulse duration is about 100-150 fs for a given laser as the tradeoff between the acceleration time and acceleration gradient[31]. To find out the crucial parameter between duration and intensity, we carried out a series of simulations by varying the pulse duration from 5 fs to 2 ps while keeping the laser energy constant. Figure 5(a) shows the energy spectra from 150 nm Au targets at different laser intensity. The dependence of the maximum energy of Au ions on the intensity is presented in Fig. 5(b). The results indicate that the laser intensity is more crucial for the acceleration of Au ions over the pulse duration, even when the pulse duration is as short as 5 fs in the case of $a_0 = 120$, which is very different from the result of low- Z ions. The use of double-layer targets leads to the prolongation of the acceleration time without sacrificing the acceleration field strength, which is highly favorable for SHI acceleration.

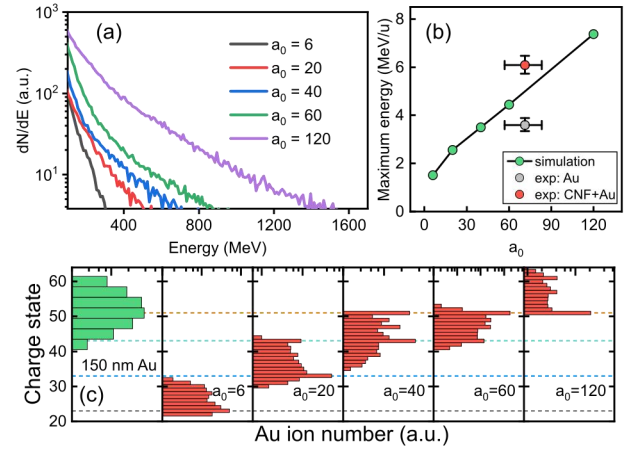


FIG. 5. (a) Energy spectra of Au ions at different intensity controlled by changing the pulse duration while keeping the laser energy constant. (b) Dependence of the maximum Au ion energy on laser intensity. The star symbols mark the experimental results. (c) The charge distribution of Au ions in experiment (green bars) and PIC simulations (red bars).

In the simulations, we find that the CSD of Au ions is closely related to the laser intensity. Fig. 5(c) exhibits the CSD of Au ions obtained in the simulations (red bars) at different laser intensities for a 150-nm Au target. The statistics include ions with energy higher than 10% of the maximum energy and within 10 degrees (half-angle) from the target normal. With the increase of the intensity from $a_0 = 6, 20, 40$ to 60 , the peak of charge states varies among Au^{23+} , Au^{33+} , Au^{43+} , and Au^{51+} , respectively. Such abundant concentration is due to the leap of the ionization energy. By comparing the experimental CSD with simulation results, an estimation of acceleration field strength, and furthermore, the on-target laser intensity, can be performed[32]. Fig.5(c) shows that the experimental CSD has an intermediate distribution between the simulated results of $a_0 = 60$ and $a_0 = 120$, which is in good agreement with the laser intensity employed in this experiment. The experimental result

of the similar CSD for single-layer and double-layer targets in Figs. 3(f) and 3(g) supports the simulation results, where the maximum acceleration fields in the two cases are close to each other. It is interesting to notice that the highest charge state presented here is 61+ (Ar-like Au), which is significantly lower than the recently reported value of 72+ in collisional ionization dominated laser-plasma interaction at the intensity of 3×10^{21} W/cm² [33]. This fact implies that the CSD obtained with collisionless ionization can be a measure of the acceleration field and consequently the on-target laser intensity.

In conclusion, we successfully realize the generation of deeply ionized Au ions up to 1.2 GeV by using ultra-intense femtosecond laser pulses. The charge state distribution, measured by our novel method, was used to analyze the acceleration process with the help of simulations. It's found that the energies of the Au ions predominantly depend on the laser intensity over the pulse duration. The use of NCD double-layer targets significantly increases the duration of the acceleration field without sacrificing the acceleration field strength. With the on-going advance in the laser intensity beyond 10^{23} W/cm², the generation of 10s GeV super-heavy ions would be realistically expected by following the scheme we demonstrated, which will pave the way to highly charged super-heavy ion beams for numerous applications.

The work was supported by the Institute for Basic Science, Korea under the project code, IBSR012-D1, NSFC innovation group project (11921006), National Grand Instrument Project(2019YFF01014402), Natural Science Foundation of China (Grant No. 11775010,11535001, 61631001) and Beijing outstanding young scientist Program. The PIC code EPOCH was in part funded by the United Kingdom EPSRC Grants No. EP/G054950/1, No. EP/G056803/1, No. EP/G055165/1, and No. EP/M022463/1. The simulations are supported by High-performance Computing Platform of Peking University.

* wenjun.ma@pku.edu.cn

¶ iwchoi@gist.ac.kr

† x.yan@pku.edu.cn

‡ chnam@gist.ac.kr

[1] N. P. Dover *et al.*, Phys Rev Lett **124**, 084802 (2020).

[2] J. Braenzel, A. A. Andreev, K. Platonov, M. Klingsporn, L. Ehrentraut, W. Sandner, and M. Schnurer, Physical Review Letters **114** (2015).

[3] L. Willingale *et al.*, Phys Rev Lett **96**, 245002 (2006).

[4] M. Nishiuchi *et al.*, Physics of Plasmas **22** (2015).

[5] J. Domański, J. Badziak, and M. Marchwiany, Laser Part Beams **36**, 507 (2019).

[6] J. Li *et al.*, New Journal of Physics **21** (2019).

[7] D. Habs, P. G. Thirolf, M. Gross, K. Allinger, J. Bin, A. Henig, D. Kiefer, W. Ma, and J. Schreiber, Applied Physics B **103**, 471 (2010).

[8] S. E. Woosley, Nature Physics **3**, 832 (2007).

[9] S. Busold *et al.*, Sci Rep **5**, 12459 (2015).

[10] D. Jung *et al.*, Physics of Plasmas **20**, 083103 (2013).

[11] S. Palaniyappan, C. Huang, D. C. Gautier, C. E. Hamilton, M. A. Santiago, C. Kreuzer, A. B. Sefkow, R. C. Shah, and J. C. Fernandez, Nat Commun **6**, 10170 (2015).

[12] M. Nishiuchi *et al.*, Physical Review Research **2** (2020).

[13] W. J. Ma *et al.*, Physical Review Letters **122** (2019).

[14] E. Clark *et al.*, Physical Review Letters **85**, 1654 (2000).

[15] F. H. Lindner, E. McCary, X. Jiao, T. M. Ostermayr, R. Roycroft, G. Tiwari, B. M. Hegelich, J. Schreiber, and P. G. Thirolf, Plasma Physics and Controlled Fusion **61** (2019).

[16] B. M. Hegelich *et al.*, Nature **439**, 441 (2006).

[17] K. V. Safronov, S. A. Gorokhov, V. A. Flegentov, A. V. Potapov, D. S. Gavrilov, A. G. Kakshin, E. A. Loboda, and D. A. Vikhlyayev, Physics of Plasmas **25** (2018).

[18] G. M. Petrov, C. McGuffey, A. G. R. Thomas, K. Krushelnick, and F. N. Beg, Physics of Plasmas **23** (2016).

[19] G. M. Petrov, C. McGuffey, A. G. R. Thomas, K. Krushelnick, and F. N. Beg, Plasma Physics and Controlled Fusion **59** (2017).

[20] D. Kawahito and Y. Kishimoto, Physics of Plasmas **27** (2020).

[21] J. Li, A. V. Arefiev, S. S. Bulanov, D. Kawahito, M. Bailly-Grandvaux, G. M. Petrov, C. McGuffey, and F. N. Beg, Sci Rep **9**, 666 (2019).

[22] C. N. Danson *et al.*, High Power Laser Science and Engineering **7** (2019).

[23] J. Domański and J. Badziak, Phys Lett A **382**, 3412 (2018).

[24] J. W. Yoon, C. Jeon, J. Shin, S. K. Lee, H. W. Lee, I. W. Choi, H. T. Kim, J. H. Sung, and C. H. Nam, Optics Express **27** (2019).

[25] J. H. Sung *et al.*, Opt Lett **42**, 2058 (2017).

[26] J. F. Ziegler, M. D. Ziegler, and J. P. Biersack, Nuclear Instruments and Methods in Physics Research Section B: Beam Interactions with Materials and Atoms **268**, 1818

(2010).

[27] T. D. Arber *et al.*, Plasma Physics and Controlled Fusion **57**, 113001 (2015).

[28] J. Q. Yu, W. J. Ma, C. Lin, and X. Q. Yan, Plasma Physics and Controlled Fusion **60** (2018).

[29] M. Ammosov, N. Delone, V. Krainov, A. Perelomov, V. Popov, M. Terent'ev, G. L. Yudin, and M. Y. Ivanov, Sov. Phys. JETP **64**, 26 (1986).

[30] J. H. Posthumus, Reports on Progress in Physics **67**, 623 (2004).

[31] J. Schreiber *et al.*, Phys Rev Lett **97**, 045005 (2006).

[32] M. F. Ciappina, S. V. Popruzhenko, S. V. Bulanov, T. Ditmire, G. Korn, and S. Weber, Physical Review A **99** (2019).

[33] R. Hollinger *et al.*, Nature Photonics (2020).